Vortex depinning as a nonequilibrium phase transition phenomenon: Scaling of current-voltage curves near the low and the high critical-current states in $2H$-NbS_2 single crystals

Biplab Bag, Dibya J. Sivananda, Pabitra Mandal,* and S. S. Banerjee†
Department of Physics, Indian Institute of Technology, Kanpur, Kanpur 208016, Uttar Pradesh, India

A. K. Sood
Department of Physics, Indian Institute of Science, Bengaluru 560012, India

A. K. Grover‡
Department of Condensed Matter Physics and Materials Science, Tata Institute of Fundamental Research, Mumbai 400005, India

(Received 15 November 2017; revised manuscript received 12 February 2018; published 12 April 2018)

The vortex depinning phenomenon in single crystals of $2H$-NbS_2 superconductors is used as a prototype for investigating properties of the nonequilibrium (NEQ) depinning phase transition. The $2H$-NbS_2 is a unique system as it exhibits two distinct depinning thresholds, viz., a lower critical current I_c^l and a higher one I_c^h. While I_c^l is related to depinning of a conventional, static (pinned) vortex state, the state with I_c^h is achieved via a negative differential resistance (NDR) transition where the velocity abruptly drops. Using a generalized finite-temperature scaling ansatz, we study the scaling of current (I)–voltage (V) curves measured across I_c^l and I_c^h. Our analysis shows that for $I > I_c^l$, the moving vortex state exhibits Arrhenius-like thermally activated flow behavior. This feature persists up to a current value where an inflexion in the IV curves is encountered. While past measurements have often reported similar inflexion, our analysis shows that the inflexion is a signature of a NEQ phase transformation from a thermally activated moving vortex phase to a free flowing phase. Beyond this inflection in IV, a large vortex velocity flow regime is encountered in the $2H$-NbS_2 system, wherein the Bardeen-Stephen flux flow limit is crossed. In this regime the NDR transition is encountered, leading to the high I_c^h state. The IV curves above I_c^h we show do not obey the generalized finite-temperature scaling ansatz (as obeyed near I_c^l). Instead, they scale according to the Fisher's scaling form [Fisher, Phys. Rev. B **31**, 1396 (1985)] where we show thermal fluctuations do not affect the vortex flow, unlike that found for depinning near I_c^l.

DOI: 10.1103/PhysRevB.97.134510

I. INTRODUCTION

Equilibrium phase transitions are characterized by breaking of a particular symmetry, for e.g., continuous translational or rotational symmetry, below a critical transition point, like the critical transition temperature [1]. The transition is characterized by an order parameter developing as the control parameter (for example, temperature) is reduced below the critical point (critical transition temperature). Another characteristic of the equilibrium critical phenomenon is scaling of quantities across the critical point [2–4]. Systems driven away from equilibrium exhibit rich features like development of self-organized states, patterns, and unusual dynamics [5–7]. Unlike equilibrium transitions a similar pedagogy isn't well established for studying nonequilibrium (NEQ) phase transitions and therefore is a topic of ongoing research [8,9]. A widely studied NEQ phenomenon is depinning [10] which is seen in diverse systems, like in driven charge density waves (CDWs) [11], Wigner crystals, magnetic domain-wall motion [12], two-dimensional colloidal systems [13,14] vortices in superconductors [10,15–17], etc. Driven two-dimensional (2D) systems exhibit a variety of out-of-equilibrium phases. Under the influence of periodic shearing forces 2D colloidal systems exhibit irreversible dynamics where the system self-organizes into either fluctuating (with collisions) or quiescent (collisions avoided) phase [18–22]. Further, the driven 2D systems exhibit the plastic depinning phenomenon with channels of mobile particles distributed between regions with localized particles [13,14,23].

We use the vortex depinning phenomenon found in type-II superconductors to study NEQ phase transitions. The vortex state in superconductors is driven from a static to a free flowing phase with a current (I) sent across a superconductor due to a Lorentz force ($\vec{F} = \vec{I} \times \vec{B}$) acting on the vortices. However, in realistic superconductors only above a threshold critical current $I = I_c$, where the magnitude of F equals the force with which vortices are pinned, viz., beyond $F = F_c$, vortices are depinned. The moving vortices [each possessing magnetic flux quanta (ϕ_0) $= 2.07 \times 10^{-7}$ G cm^2] generate a voltage (V) drop along the direction of current flow. For an application point of view, it is important to pin these vortices strongly so that superconductors carry current without generating any dissipation due to vortex motion (viz., maintain a $V = 0$ state in the presence of a current). The vortex velocity (u) is proportional to V

*Present address: Narasinha Dutt College, Howrah 711101, West Bengal, India.
†Corresponding author: satyajit@iitk.ac.in
‡Present address: Department of Physics, Panjab University, Chandigarh 160014, India.

as $V = uBd$, where d is the spacing between voltage contacts. By measuring the current (I)–voltage (V) characteristics one can study the drive (F)–velocity (u) relationship for the driven vortex state [16]. The moving vortex state is treated like an elastic manifold driven through a random pinning environment provided by the disorder in the superconductor. At low drives (low u, just above the critical current), vortex depinning can be either elastic or plastic. During elastic depinning the entire vortex state depins simultaneously [17]. In plastic depinning, channels of vortex motion are created around islands of pinned vortices [15,16,24]. At higher drives (high u) the moving vortex state driven across the pinning environment exhibits different phases. At high vortex velocities averaging over disorder leads to a recrystallization of the vortex state, producing a drive induced ordering of the moving vortex phase [25]. It was shown that the averaging over disorder is preferentially along the direction of motion, producing a coupled channel-like flow of vortices, viz., a moving Bragg glass phase which is free of topological defects [26]. Apart from a moving Bragg glass phase, one also encounters a smectic phase with vortex motion along decoupled channels [27,28].

Various studies have been undertaken to characterize such NEQ phases and transitions between them. One route has been to study effects of critical fluctuations on the vortex dynamics [29]. Here one investigates the vortex dynamics in a critical fluctuation regime close to T_c where thermal fluctuation effects are significant. In our paper we investigate the vortex dynamics over a wide temperature range which are far away from T_c, and hence we analyze the data using alternate schemes. At $T = 0$ K, it is expected that as the vortex state depins, u rises abruptly from zero at $F = F_c$ and subsequently increases at $F > F_c$ [15,16]. Here the depinning transition looks like a phase transition. Akin to an equilibrium critical transition, Fisher theoretically investigated this NEQ depinning phenomenon with a control and order parameter [30]. As per Fisher's proposal, for a vortex depinning transition, the mean vortex velocity (u) is the order parameter since u develops at $F \geqslant F_c$ and the control parameter is the reduced driving force $f = \frac{F-F_{c0}}{F}$, where $F_c|_{T=0\mathrm{K}} = F_{c0}$ is the zero-temperature critical depinning force. Here F_{c0} is analogous to the concept of a critical point in equilibrium transitions. At $T = 0$ K, Fisher described the sharp NEQ depinning transition at F_{c0} with a dynamic critical exponent β [30], viz.,

$$u \propto \left(1 - \frac{F_{c0}}{F}\right)^{\beta}. \tag{1}$$

Equation (1) has been proposed in other theoretical studies as well [31]. While Eq. (1) is valid at 0 K, a more general ansatz incorporating the effects of thermal fluctuations at finite T was proposed [32],

$$u \propto T^{1/\delta} S[T^{-1/\beta\delta} f]. \tag{2}$$

In Eq. (2), S is a scaling function which is proposed to behave as $S(x) - S(0) \sim x^{\beta}$ at $x \to 0^+$ (i.e., for $F \to F_{c0}^+$, viz., F approaching F_{c0} from above) and for $F < F_{c0}$, i.e., $x < 0$, $S(x) \sim \exp(U_c x)$, an exponential function, where U_c is the bare pinning potential. Note that scaling forms like Eqs. (1) and (2) are not restricted to the study of depinning of vortices, but for any depinning transition. In fact recent numerical studies show that Eq. (2) describes the velocity-drive relationship at finite T, for not only depinning vortices in superconductors [32,33] but also depinning of magnetic domain walls in two-dimensional (2D) magnetic films [34]. In these numerical simulations of domain-wall motion in 2D magnetic films, the scaling function of Eq. (2) is used to study the critical domain-wall depinning transition and the associated critical exponents.

Experiments on driven vortex state in 2D amorphous superconducting Mo_xGe_{1-x} thin films (330 nm thick) [35] have confirmed that isofield (fixed B varying T) IV's scale obeying Eq. (2). However, there are certain unexplored issues which remain to be resolved: Equation (2), originally proposed for a three-dimensional system, while shown to be valid also for thin films [35], has not been verified in thick three-dimensional (3D) single crystals. Furthermore, recently it has been shown that single crystals of a chalcogenide superconductor $2H$-NbS_2 exhibit two distinct vortex depinning phenomena occurring at the same field and temperature [36,37]. In these single crystals, after depinning from a relatively low I_c state (at I_c^l) the vortex state is driven into a high velocity dissipating state at large I. Here it is found that, the vortex velocity abruptly drops to a low value via a negative differential resistance (NDR) transition [37]. This driven state depins at a higher I_c, viz., $I_c^h > I_c^l$ [37] and the depinning from I_c^h is unconventional with unique voltage fluctuation properties [37]. Here we study the IV scaling properties near I_c^l and I_c^h in two single crystals of $2H$-NbS_2 with different pinning strengths. We show that above I_c^l the isofield IV curves obey the 3D scaling ansatz of Eq. (2). From the scaling of IV's we show that at $I > I_c^l$ there is a thermally activated regime which extends to the knee in IV, viz. till $I = I_{\mathrm{cr}}$, and we also determine the pinning strength (U_c) in these crystals. We identify the knee in IV's ($I = I_{\mathrm{cr}}$) as a drive regime where there is an NEQ transformation from thermally activated to free flow vortex motion. The dynamic scaling exponents associated with the critical depinning transition at I_c^l are shown to be weakly affected by sample pinning strength but are sensitive to dimensionality of the vortex state. From our study we also propose a modification to the scaling ansatz of Eq. (2) to analyze isothermal IV's which heretofore did not exist. Interestingly, the IV's above I_c^h do not scale as per the ansatz of Eq. (2). In fact, the scaled IV's above I_c^h are found to obey the classic Fisher's form, Eq. (1) [30]. Our study shows that the temperature is not a relevant scaling quantity in this regime. Therefore, we report that increased thermal fluctuations at high T do not reduce the high I_c^h of the state generated from vortex flow instabilities at high current drives. Such a feature has not been found for a conventionally pinned vortex in which thermal fluctuations always produce an effective reduction of the pinning potential. Based on our analysis we show that an NDR generates flow instabilities creating a unique high I_c^h state, which behaves like a disordered vortex state and possesses significant rigidity against thermal fluctuations and drive. The validity of Fisher's scaling and the abrupt depinning near I_c^h give it an impression of coherent depinning of a rigid elastic medium which resists thermal fluctuation effects, despite it being a disordered vortex configuration.

TABLE I. Details of the sample.

Sample	T_c (K)	RRR = R(300)/R(10)	d (mm)	α	I^l_{c0} (mA)	δ	β_l[a]	β_h	U_c
A1	5.8 ± 0.1	25	0.53 ± 0.03	0.6	26.5 ± 0.1	2.56 ± 0.05	0.39 ± 0.01	0.88 ± 0.09	19.74 ± 0.22
A2	5.8 ± 0.1	35	0.30 ± 0.02	0.9	18.5 ± 0.2	2.38 ± 0.09	0.42 ± 0.02	0.88 ± 0.06	10.78 ± 0.16

[a]Corresponding to $\beta_l \delta = 1$.

II. SAMPLE AND EXPERIMENTAL DETAILS

We use the four-probe technique to study transport properties in two single crystals of $2H$-NbS_2 superconductors (we label them as samples A1 and A2). The single crystals were grown using the standard vapor transport technique; the details of growth are given elsewhere [38]. Dimension of these samples are, A1: $2.0 \times 1.0 \times 0.045$ mm^3, A2: $0.9 \times 0.9 \times 0.045$ mm^3. Samples A1 and A2 used in the present study have also been investigated earlier [36,37]. Although the samples have a similar T_c, their residual resistivity ratios [RRR $\equiv$ R(300 K)/R(10 K)] are different: A1 and A2 have a RRR of 25 and 35, respectively. The physical dimensions, T_c, and RRR for the two rectangular shaped samples (cut using razor blades) are listed in Table I. Four-probe contacts were made on freshly cleaved surfaces of the samples using low-temperature silver epoxy. We obtained a contact resistance of 10 mΩ. To minimize the effects of current flowing primarily along the edges, the contacts were made away from the edges and near the middle of the sample. The features in IV data reported in this paper are independent of whether the samples were zero-field cooled (ZFC) or field cooled (FC). Here, the IV curves shown are for the samples prepared with ZFC thermomagnetic history with the dc magnetic field applied in a no-overshoot mode [for comparison Sec. (i) of the Supplemental Material [39] shows the IV curves recorded on samples prepared with FC history]. From the IV measurements, we determine the threshold depinning current (I_c) using the criteria that the mean voltage $\langle V \rangle$ exceeds 2 μV when $I \geqslant I_c$. In our experiments, I flows in the basal (ab) plane of the single crystals and B is applied along the crystallographic c axis of the crystals ($B \parallel c$). Using $V = Bud$, where d is the distance between the voltage contacts (cf. Table I), we estimate the mean u for the drifting vortices. For example, in A1, $V = 40\,\mu$V at $B = 0.7$ T corresponds to $u \sim 11$ cm/s. Note in Refs. [36,37,40], from bulk magnetization and transport measurements, we had already observed the bulk 3D collective pinning character in samples A1 and A2. Earlier studies of field dependence of the critical current in these samples indicated the presence of collective weak pinning [41,42].

III. DEPINNING CHARACTERISTICS ACROSS TWO DEPINNING THRESHOLDS, I^l_c and I^h_c

Figure 1(a) (main panel) shows the isothermal IV (viz., IV's measured at fixed T for zero-field-cooled (ZFC) vortex states with different densities prepared at different B) of a driven vortex state in sample A1 at 2.5 K, in the low current regime [for better identification of the critical currents, we have replotted Figs. 1(a) and 1(b) with the V axis in log scale in the Supplemental Material, Sec. (ii) [39]]. It shows that, at 0.2 T and 2.5 K, the vortices depin from a static pinned state at $I^l_c \sim$ 24 mA (marked by the arrow), after which the IV exhibits a concave curvature followed by a knee at $I_{\rm cr} \sim 34$ mA [see Fig. 1(c) inset to identify the location of the knee at $I_{\rm cr}$]. Above $I_{\rm cr}$ the IV is linear. The isothermal IV response in the low current regime for sample A2 exhibits almost similar features [see Fig. S3(a), section (iii) of Supplemental Material [39]]. In sample A2, the relatively low I^l_c value of 14.4 mA at 2.5 K, 0.5 T [see Fig. S3(a) in the Supplemental Material [39]] compared to 20.8 mA at the same B, T in sample A1 suggests weaker pinning in A2 compared to A1 (this is consistent with A2 having a higher RRR; see Table I). To identify that electrical transport properties aren't surface dominated, we perform magnetization hysteresis loop measurements at different fields and temperatures [see a typical hysteresis loop at 1.8 K shown in Sec. (iv) of the Supplemental Material [39]]. An asymmetric loop indicates the dominance of surface pinning over bulk pinning in the sample [43,44]. The observed symmetric nature of the magnetization hysteresis loop in sample A1 shows that surface pinning effects do not dominate and consequently, the critical currents determined here correspond to bulk pinning and transport currents flow through the bulk of the sample. Note that with increase in B, $I^l_c \propto \frac{1}{B^\alpha}$ [see Figs. 1(a) and S3(a) insets, where $\alpha = 0.6 \pm 0.1$ for sample A1 and $\alpha = 0.9 \pm 0.1$ for A2], which indicates depinning of a collectively pinned elastic vortex medium and similar features have been shown earlier [16,37,41,45]. Figure 1(b) [and S3(b)] shows the isofield IV's (viz., IV's measured at fixed B at different T after zero-field cooling) for A1 at 0.7 T (and at 0.8 T for A2). The IV features in Figs. 1(b) and S3(b) are similar to that in Fig. 1(a).

The inset of Fig. 1(c) shows that for the forward run beyond the inflexion (knee) in IV at $I_{\rm cr}$, the voltage or vortex velocity increases almost linearly with the driving force (i.e., I), suggesting a steady-state flow of the driven vortex state. This steady flow state with large vortex velocities is sustained up to 60 mA after which the voltage values abruptly drop [cf. Fig. 1(c) inset] due to the onset of a negative differential resistance (NDR) transition [46–52] (we will discuss NDR in later sections). For all our measurements, the temperature fluctuations close to the sample holder at different I were stable to within 5 mK [see Sec. (v) of the Supplemental Material [39]]. After reaching 90 mA, the current is ramped down to zero while measuring IV (reverse IV run). In this reverse IV run, the voltage exhibits fluctuation and falls below the noise floor as I is reduced below a critical value of $I^h_c \sim 45$ mA. Infact, after this reverse run, without changing B and T when the forward IV measurement is repeated by increasing I (data not shown), then vortex depinning occurs only above I^h_c and this is true for all subsequent repeated IV's performed, i.e., depinning from I^l_c is never recovered [37]. From Fig. 1(c) inset note that at 0.2 T and 2.5 K, the depinning features above the higher critical current ($I^h_c \sim 45$ mA) is completely different from that above $I^l_c = 24$ mA. Hence after the NDR

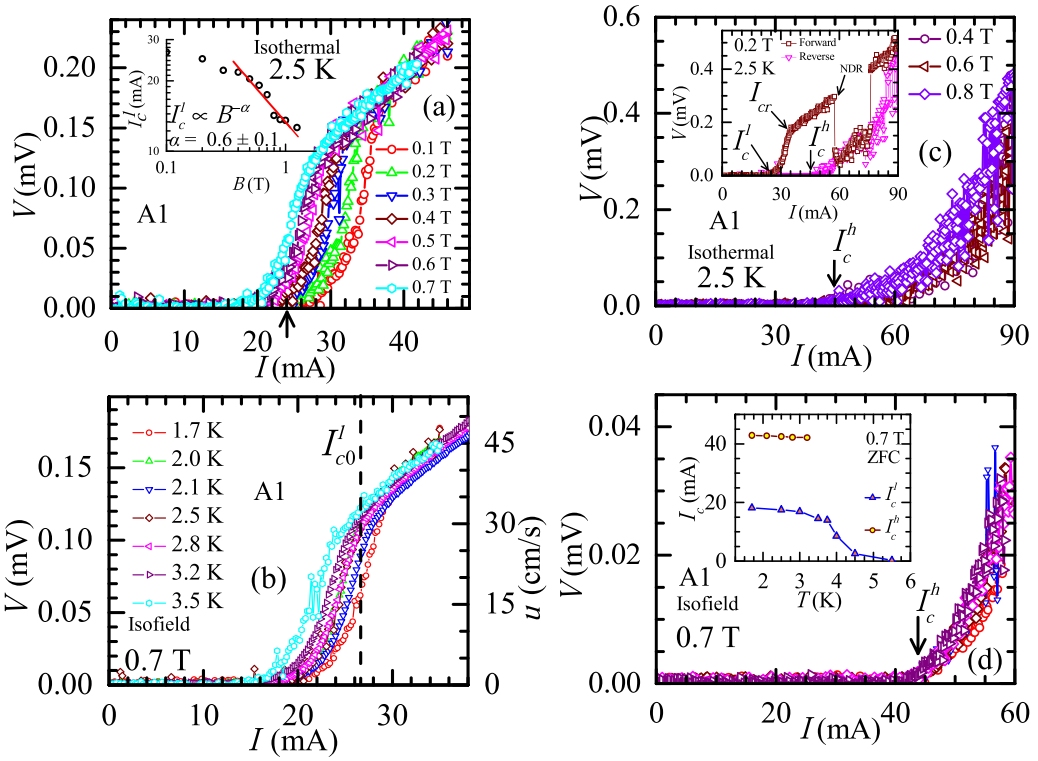

FIG. 1. (a) Isothermal *IV* response for ZFC state around I_c^l at 2.5 K for sample A1 with $B = 0.1, 0.2, 0.3, 0.4, 0.5, 0.6$, and 0.7 T. The arrow locates the I_c^l value for the *IV* curve at 0.2 T in sample A1. The inset of (a) shows the *B* dependence of I_c^l for sample A1 at 2.5 K. (b) The isofield *IV* curves for ZFC state around I_c^l at 0.7 T with $T = 1.7, 2.0, 2.1, 2.5, 2.8, 3.2$, and 3.5 K for sample A1. The location of I_{c0}^l [determined from Fig. 2(a)] is identified with vertical dashed line in (b). In (a) and (b) the *IV* has been recorded (with increasing current) after preparing the static vortex state in ZFC, with field set in no-overshoot mode. Panels (a) and (b) are replotted on a log-linear scale in the Supplemental Material, Sec. (ii), to identify the critical current clearly. (c) Isothermal *IV* characteristics (ZFC) across I_c^h measured at 2.5 K and $B = 0.4$, 0.6, and 0.8 T. The inset of (c) shows the *IV* curves for the forward and reverse runs in sample A1 at 2.5 K and 0.2 T. The locations of I_c^l, I_{cr}, I_c^h and onset of NDR have been identified with arrows in inset (c). (d) The main panel shows the isofield *IV* curves for sample A1 at 0.7 T and $T = 1.7$, 2.1, 2.5, 2.8, and 3.2 K (ZFC). The temperature labels are similar in (b) and (d). In (c) and (d) primarily we have reached the high I_c state by cycling current [as shown in Fig. 1(c) inset] and after that the *IV* is recorded while increasing current. Inset of (d) shows *T* dependence of I_c^l and I_c^h at 0.7 T for ZFC state in sample A1. The locations of I_c^h are identified by arrows in (c) and (d).

transition, the driven vortex state transforms into a stable high I_c state which depins above I_c^h. [Note that Fig. 5(b) where the *IV* (at 0.7 T) is plotted as resistivity versus *I* shows that at the NDR transition close to 40 mA the vortex flow abruptly slows down and the velocity drops below the noise floor. This state depins from a higher I_c^h.] Figures 1(c) and 1(d) show the isothermal (at 2.5 K) and isofield (at 0.7 T) depinning (*IV*) characteristics for sample A1 across I_c^h. [For these sets of data, we first reach the high I_c state by cycling the current (a procedure which is similar to Fig. 1(c) inset) and then we record the *IV* as the current is increased from zero.] We observe in Figs. 1(c) and 1(d) that unlike the smooth depinning above I_c^l, the *IV* response above I_c^h is very noisy and the fluctuations are sustained up to large drives. Further, unlike the $I_c^l \propto \frac{1}{B^\alpha}$ behavior as shown in Fig. 1(a) inset, in Fig. 1(c) we observe that for all magnetic fields the *IV*'s depin almost at the same current values, suggesting that I_c^h is independent of *B*. Figure 1(d) inset shows the *T* dependence of I_c^l and I_c^h for sample A1 at 0.7 T. It shows that with increasing *T* there is monotonous suppression in the I_c^l values due to thermal fluctuation induced smearing of the pinning potential [15] whereas the $I_c^h(T)$ values are almost *T* independent. Hence, we observe that in sample A1, unlike the behavior of I_c^l, I_c^h is almost constant irrespective of variations in *B* or *T*. This implies I_c^h is not affected by intrinsic pinning variations in the sample. In Ref. [37] we had shown that I_c^h is also not correlated with RRR variations in the sample. Furthermore, the fact that I_c^h is almost independent of *B* [see Figs. 1(c) and also Fig. 1 of Ref. [37]] suggests it is not related to underlying transformation in the static vortex lattice [for details see Sec. (iv) of the Supplemental Material [39] and Ref. [53]]. Based on these arguments, we argue that depinning from the higher critical-current state I_c^h is unconventional and unlike conventional depinning at I_c^l. As mentioned earlier [see Sec. (i) of the Supplemental Material [39]], we don't observe any significant difference between the *IV* curves for the vortex states prepared with ZFC or FC thermomagnetic histories. We find that I_c^l and I_c^h values are almost identical for ZFC and FC states [see Fig. S1(b), inset, in Sec. (i) of the Supplemental Material [39]].

Note that during our measurements the sample temperature is almost uniform with negligible heating effects. Our earlier investigations (on the same samples) of time series of the voltage [$(V(t)$] generated from the moving vortex state driven by constant current [see Figs. 3(a)–3(c) of Ref. [36] and

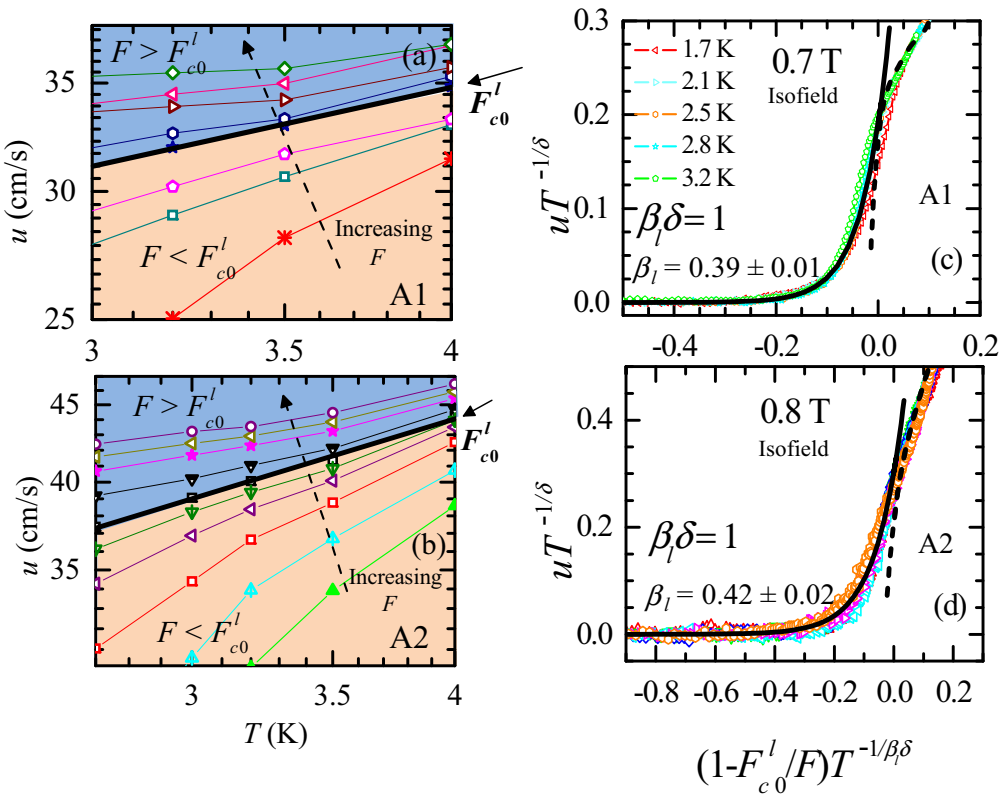

FIG. 2. Panels (a) and (b) show $u(T)$ response in log-log scale for sample A1 (with $F = 17.2$, 17.9, 18.2, 18.6, 18.9, 19.3, 19.6, and 20.2 mA T) and sample A2 (with $F = 12.8$, 13.4, 14.0, 14.6, 14.8, 15.0, 15.4, 15.5, and 15.7 mA T) estimated from *IV*'s in Figs. 1(b) and S3(b) respectively. The dashed arrows indicate the increasing order of F. The $F < F^l_{c0}$ and $F > F^l_{c0}$ regimes are shown with different shading. The thick black straight line represents the $u(T)$ response at $F = F^l_{c0}$. (c) $uT^{-1/\delta}$ vs $(1 - \frac{F^l_{c0}}{F})T^{-1/\beta_l\delta}$ curves at 0.7 T with different T for sample A1 plotted using $F^l_{c0} = 18.6$ mA T, $1/\delta = 0.39$, $\beta_l\delta = 1$ and $\beta_l = 0.39$. (d) $uT^{-1/\delta}$ vs $(1 - \frac{F^l_{c0}}{F})T^{-1/\beta_l\delta}$ at 0.8 T for sample A2 with $\beta_l\delta = 1$. The scaling parameters are $F^l_{co} = 14.8$ mA T, $1/\delta = 0.42$, and $\beta_l = 0.42$. The black continuous and dashed curves in (c) and (d) are fit to Eqs. (4) and (3) respectively. The T legend shown in (c) is the same for (d).

Figs. 1(f) and 2(c) (inset) of Ref. [37]] showed a uniform mean voltage level, $\langle V \rangle$ maintained over sufficiently long time intervals (over tens of minutes). Heating effects would have caused a smearing and weakening of the pinning in the sample, and the mean vortex velocities in the $V(t)$ would have increased with heating effects rather than remain uniform over a significant interval of time. Since these time intervals (> few tens of minutes) over which the mean $\langle V \rangle$ remains uniform are much longer than the typical time intervals over which we measure our *IV* characteristics (∼ few minutes), heating from the contacts isn't responsible for the features reported in our measurements. The high I_c state is produced from a fast flowing vortex state achieved with high driving current. We find that at high temperatures close to T_c there is a significant thermal runaway effect at high drives, due to which we are unable to maintain constant sample temperature during the measurement. Due to this limitation we have reported results on I^h_c at low T ($\leqslant$3.2 K) where we are able to maintain a uniform sample temperature during the measurements.

IV. DETERMINING F_{c0} AND THE DYNAMIC EXPONENTS

In order to study scaling of the isofield *IV*'s above I^l_c [see Fig. 1(b)] using Eq. (2), we first determine the exponent δ and F_{c0} following the procedure in Refs. [32,33]. Note that for sample A1 in Fig. 1(b) [see Fig. S3(b) in the Supplemental Material [39] for sample A2] the y axis on the right-hand side of these plots has the voltage converted to vortex velocity u (using $V = Bud$). In Fig. 1(b) [and Fig. S3(b) in the Supplemental Material [39]] at a constant value of I (or driving force F), u increases monotonically with T, for e.g., at a constant $I = 22$ mA, Fig. 1(b) shows u changes from ∼2 cm/s to ∼18 cm/s as T increases from 1.7 to 3.5 K. Figure 2(a) shows the u vs T curves (in log-log scale) determined from the *IV* curves in Fig. 1(b) at different fixed values of the driving force F (or fixed I values), as outlined above. It shows that as F is increased, there is a change in the curvature of $u(T)$ from convex (at low values of F) to concave (at higher F). In Fig. 2(a) these two regimes are represented with different color shades. From Fig. 2(a) one observes that the curves change shape as F approaches an intermediate drive value of $F = F^l_{c0} = 18.6 \pm 0.1$ mA T. The $u(T)$ response is a straight line (on a log-log scale), viz., $u \propto T^{1/\delta}$ at $F = F^l_{c0}$ [note that Eq. (2) suggests $u \propto T^{1/\delta}$ behavior at $F = F_{c0}$). The thick black line in Fig. 2(a) is a fit to the equation $u \sim T^{1/\delta}$ yielding a $1/\delta$ value of 0.39 ± 0.01 (for sample A1). For A1, the F^l_{c0} value of 18.6 mA T corresponds to a zero-temperature critical depinning current $I^l_{c0}(= \frac{F^l_{c0}}{B}) = 26.6$ mA, whose location is

marked via the vertical dashed line in Fig. 1(b). Note from Fig. 1(b) that I^l_{c0} is located very close to the knee (inflexion) in the *IV* curve, viz., at I_{cr}. In Fig. 2(b), a similar analysis for A2 gives $F^l_{c0} = 14.8 \pm 0.1$ mA T or $I^l_{c0} = 18.5$ mA. The value of $1/\delta$ (slope of the u-T curve) is 0.42 ± 0.02 for sample A2. As the pinning for sample A1 is larger than sample A2, the I^l_{c0} values are also correspondingly larger (see the comparison of I^l_{c0} and δ in Table I for A1 and A2). From Table I we note that the exponent δ, which controls how u changes with thermal fluctuations, is almost insensitive to the variation in RRR and I^l_{c0}, viz., pinning strength, across the two samples. The typical value of δ in our $2H$-NbS_2 single crystals is ~2.3–2.6, while that in the MoGe thin films is quite different, viz., it is ~0.28 [35]. The critical-current density J_c of our $2H$-NbS_2 samples is $\sim 40\,\mathrm{A\,cm^{-2}}$ which is comparable to $J_c \sim 50\,\mathrm{A\,cm^{-2}}$ of their MoGe films [35]. Note that the thickness of our single crystals is ~130 times the MoGe film thickness (~330 nm). We would like to mention that it was difficult to achieve significant in-sample thickness variation by cleaving the $2H$-NbS_2 crystals, as repeated cleaving was introducing microcracks and nonuniform steps on the sample surface, therefore we couldn't compare our results across $2H$-NbS_2 samples with significantly different thickness. Alternatively, for a comparison of our results we chose MoGe film results. We believe the scaling feature associated with such NEQ depinning transitions is a property independent of the type of material chosen. We see that although pinning strengths across our $2H$-NbS_2 crystals and the MoGe thin films are roughly comparable, there is a significant change in the scaling parameters. This suggests that dimensionality of the sample may be affecting the scaling parameters. Exploring the thickness dependence of the scaling analysis is worthwhile for future studies as it may help to unravel the features of the underlying universality class governing the scaling behavior of such NEQ transitions.

V. SCALING OF *IV* CURVES AT DIFFERENT *T* AT FIXED *B*, ACROSS I^l_c (ISOFIELD DATA SCALING)

In Figs. 2(c) and 2(d), the isofield *IV* curves measured at different T [Figs. 1(b) and S3(b) [39]] were replotted in terms of scaled variables, $y = uT^{-1/\delta}$ and $x = (1 - F^l_{c0}/F)T^{-1/\beta_l\delta}$ with $\beta_l\delta = 1$(the subscript l identifies the β parameter is related to I^l_c) for sample A1 and A2 respectively. In Fig. 2(c) [and 2(d)], it is clear that using the above scaled parameters, the isofield *IV* data scale onto a single curve with $\beta_l\delta = 1$ [see the scaling of curves with varying $\beta_l\delta$ in Figs. S6(a)–S6(f) in Sec. (vi) of the Supplemental Material [39]]. As δ has already been determined from Figs. 2(a) and 2(b) (see Table I), using $\beta_l\delta = 1$, we get β_l equal to 0.39 ± 0.01 and 0.42 ± 0.02 for samples A1 and A2 respectively. Note that $\beta_l\delta \sim 0.5$ was obtained for MoGe thin films (330 nm thick) [35]. As discussed earlier and also as Table I shows, the scaling exponents are insensitive to pinning; they however depend on dimensionality of the vortex state which depends on the sample thickness.

For the scaling curves in the $x > 0$ ($F > F^l_{c0}$) regime, the $y(x)$ behavior in Fig. 2(c) is fitted to a function $S(x)$ of the form [32]

$$S(x) = a_0 + a_1 x^{\beta_l}, \tag{3}$$

where $a_0 = 0.15 \pm 0.02$ and $a_1 = 0.35 \pm 0.05$ (shown by the dashed curve). Furthermore, for the $x < 0$ ($F < F^l_{c0}$) regime, the scaled $y(x)$ curves in Fig. 2(c) are fitted to a function $S(x)$ of the form [32]

$$S(x) = a_2 \exp(a_3 x), \tag{4}$$

where $a_2 = 0.19 \pm 0.01$ and $a_3 = 19.75 \pm 0.22$ (shown by a solid curve). For $x < 0$, the exponential form of $S(x)$ in Eq. (4) describes an Arrhenius-like thermally activated motion of vortices across pinning barriers of height U_c. By substituting Eq. (4) in Eq. (2) and using $\beta_l\delta = 1$ we get

$$u \propto T^{1/\delta} \exp[-U_c(1 - F_{c0}/F)/T]. \tag{5}$$

The coefficients a_3 in Eq. (4) is identified as the pinning potential U_c in Eq. (5). The fitting parameter a_3 gives $U_c \sim 19.75 \pm 0.22$ K for A1 and $U_c = 10.78 \pm 0.16$ K for A2 (see Table I). These U_c values confirm our earlier inference of sample A2 being weaker pinned than sample A1. The value of U_c hasn't been determined for the MoGe samples in Ref. [35], as their value of $\beta_l\delta \neq 1$. From the fitting to Eq. (4), we note that a thermally activated motion of vortices leads to a concave rounding of the *IV*'s in the drive regime of $I^l_c < I < I^l_{c0}$ (or I_{cr}), i.e., the thermally activated motion persists up to $I_{cr} \sim I^l_{c0}$. As vortices depin and move across a random pinning landscape, a velocity distribution develops at any given instant of time as some slowly moving vortices will display thermally activated motion across the pinning landscape while some will be moving faster. Thus in the presence of thermally activated motion the mean vortex velocity increases gradually with drive. Beyond I_{cr} as the vortices are driven hard, they glide over the pinning potentials without feeling their effects and enter a coherent flow regime. However, this coherent flow regime above I_{cr} isn't stable and an abrupt drop in u is encountered at these high velocities.

We know from Figs. 2(c) and 2(d) that above the knee (i.e., above I_{cr}) the scaled *IV* curves fit to Eq. (3) [see the dashed curves in Figs. 2(c) and 2(d)]. For $F > F^l_{c0}$, substitution of Eq. (3) in Eq. (2) yields the form

$$u \propto a_0 T^{1/\delta} + a_1 \left(1 - \frac{F^l_{c0}}{F}\right)^{\beta_l}. \tag{6}$$

From Eq. (6) we see that at $F > F^l_{c0}$, i.e., $x > 0$, the second term in the expression is Eq. (1) proposed by Fisher [30] and the first term is related to the effect of thermal fluctuations on u. It is interesting to note from the scaling analysis that I_{cr} signifies a transformation from a thermally activated flow regime obeying one scaling form [viz., Eq. (4)] for $I < I_{cr}$ ($= I^l_{c0}$) to a rapid flow regime with a distinctly different scaling form [viz., Eq. (3)] at $I > I_{cr}$. Note that Eqs. (3) and (4) are not analytically related.

VI. SCALING OF ISOTHERMAL *IV* CURVES ABOVE I^l_c

While all earlier scaling studies [32,33,35] have analyzed isofield *IV*'s, we propose here a method to scale isothermal *IV*'s as well, viz., *IV* measured at constant T at different B [cf. Figs. 1(a) and S3(a)]. Note that from the isothermal *IV*'s [32,33] we cannot determine F^l_{c0} or $u \propto T^{1/\delta}$ behavior following the procedure outlined via Figs. 2(a) and 2(b). To determine F^l_{c0}

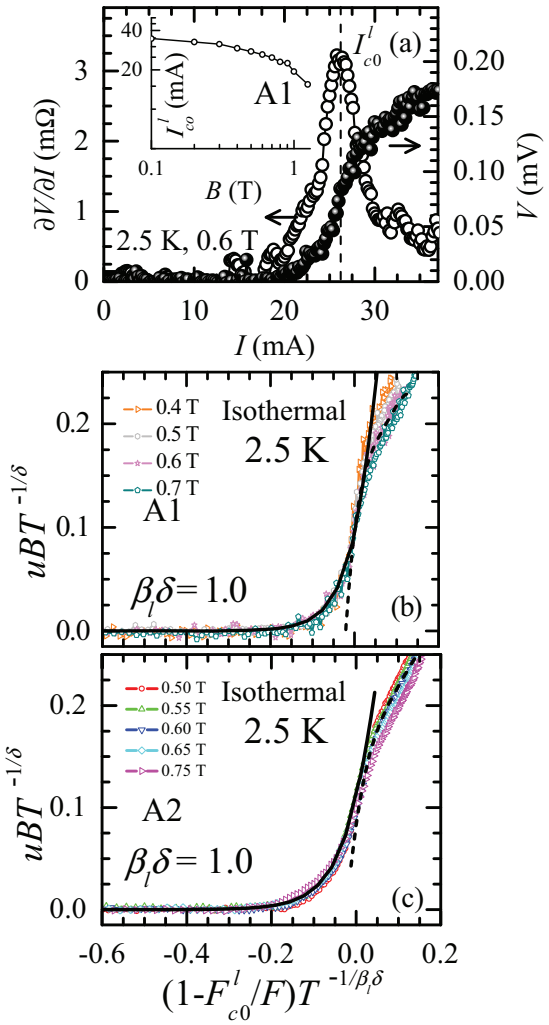

FIG. 3. (a) The right y axis shows the IV response for sample A1 at 2.5 K and 0.6 T and the left y axis presents the corresponding $\frac{\partial V}{\partial I}(I)$ response showing a peak in $\frac{\partial V}{\partial I}$ at $I \equiv I^l_{c0} = 26.17$ mA (identified by the vertical dashed line). Inset shows the I^l_{c0} against B for sample A1 in log-log scale at 2.5 K. (b),(c) Scaling plots for the isothermal IV response at 2.5 K with different B in terms of scaled variables $uBT^{-1/\delta}$ vs $(1-\frac{F^l_{c0}}{F})T^{-1/\beta_l\delta}$ at 2.5 K and different B with $\beta_l\delta = 1$ for sample A1 ($\beta_l = 0.39$) and A2 ($\beta_l = 0.42$) respectively. The black continuous and dashed curves are fit to Eqs. (4) and (3) respectively.

values in the isothermal IV data, we take recourse to the observation made in the isofield studies [see Fig. 1(b)] that the $I^l_{c0} \sim I_{\rm cr}$. In Fig. 3(a), main panel, the right-hand y axis is the voltage V while the left axis is the corresponding $\frac{\partial V}{\partial I}$, which shows a peak at the knee of the IV, viz., at $I_{\rm cr}$. Thus, using the criteria that $I_{\rm cr} \sim I^l_{c0}$, we identify F^l_{c0} or I^l_{c0} in the isothermal IV data as the peak in the derivative $(\frac{\partial V}{\partial I})$ versus I (inflexion in IV). Using these I^l_{c0} values, we attempt the scaling of the isothermal IV curves measured at different B. Note that $I^l_{c0} = 26.17$ mA at 0.60 T corresponds to $F^l_{c0} = 15.70$ mA T. Figure 3(a) inset shows the estimated $I^l_{c0}(B)$ behavior on a log-log scale.

Figures 3(b) and 3(c) show that the isothermal IV's [of Figs. 1(a) and S3(a)] at 2.5 K are scaled only by defining a slightly modified variable, $y = uBT^{-1/\delta}$, whereas $x = (1 - F^l_{c0}/F)T^{-1/\beta_l\delta}$ is same as earlier [recall Figs. 2(c) and 2(d)]. Note here we have used the fitting parameters $\beta_l\delta \sim 1$ and $\delta = 2.56 \pm 0.05$ and 2.38 ± 0.09 for A1 and A2 samples respectively [as obtained from Figs. 2(a) and 2(b)]. Based on the above analysis of isothermal IV we suggest a modified version of the scaling ansatz of Eq. (2), viz.,

$$u \propto \frac{T^{1/\delta}}{n} S[T^{-1/\beta\delta} f], \tag{7}$$

where $n = \frac{B}{\phi_0}$ is the vortex number density and ϕ_0 is the magnetic flux quantum. The difference between Eqs. (2) and (7) is the inverse relation between vortex velocity and the vortex density. The behavior of the $S(x)$ in Figs. 3(b) and 3(c) for $x > 0$ and $x < 0$ obeys Eqs. (3) and (4) respectively [similar to the behavior of scaling of the isofield IV curves in Figs. 2(c) and 2(d)]. In Figs. 3(b) and 3(c), fitting the scaled data with Eq. (5) for $x < 0$ yields $U_c \sim 19.48 \pm 0.47$ K and 13.07 ± 0.25 K for A1 and A2 respectively, which are similar to the U_c values determined above for the isofield IV data (see Table I).

VII. UNCONVENTIONAL DEPINNING AT I^h_c AND THE SCALING OF IV CURVES ABOVE I^h_c

We now investigate the depinning phenomenon from the high I_c state in these crystals. In Figs. 1(c) and 1(d), we have already shown the isothermal and isofield IV curves associated with depinning from I^h_c for sample A1. Here we analyze the scaling behavior of IV's near I^h_c. Figures 1(b) and 1(d) show that for a similar range of temperature variation at fixed magnetic field, while I^l_c shifts with T, I^h_c is almost unaffected. The shifts in IV curves near I^l_c were used to demonstrate the validity of the $u \propto T^{1/\delta}$ relationship for depinning near I^l_c (recall Fig. 2). The weak temperature dependence of the IV curves near I^h_c shows that for an I above I^h_c, the u is almost constant and unaffected by T, which implies that the $u \propto T^{1/\delta}$ relationship is not valid near I^h_c. This suggests that compared to depinning at I^l_c where vortex velocities change with T, for depinning near I^h_c the vortex velocities at $I > I^h_c$ are unaffected by thermal fluctuation effects. Furthermore, unlike the IV's above I^l_c which have an inflection at $I_{\rm cr}$ [cf. Fig. 1(c) inset], there is no such feature in the IV's above I^h_c. A noteworthy feature of Figs. 1(c) and 1(d) is that depinning at I^h_c is abrupt and sudden, unlike the gradual increase observed above I^l_c. In Figs. 4(a) and 4(b) we replot the isothermal IV data [at 2.5 K; see Fig. 1(c) for A1] for samples A1 and A2 as u versus $(1 - \frac{I^h_c}{I})$ on a log-log scale. One observes in Figs. 4(a) and 4(b) that all the curves at $I > I^h_c$ are linear and overlap onto a scaled curve of the form $u \propto (1 - \frac{F^h_{c0}}{F})^{\beta_h}$ with $\beta_h \sim 0.88 \pm 0.09$ for sample A1 and 0.88 ± 0.06 for A2 [determined from the slope of the curves in Figs. 4(a) and 4(b)]. Note that we have found that the isofield IV's above I^h_c also show similar scaling features with $\beta_h \sim 0.89 \pm 0.06$ for sample A1 [see Sec. (vii) of the Supplemental Material [39]]. The above fitting to the IV data above I^h_c corresponds to Eq. (1) describing a nonequilibrium critical depinning transition at 0 K as proposed by Fisher [30,31]. Interestingly in this high current regime (viz., $I > I^h_c$), although all our experiments have been performed at finite temperature, we see a validity

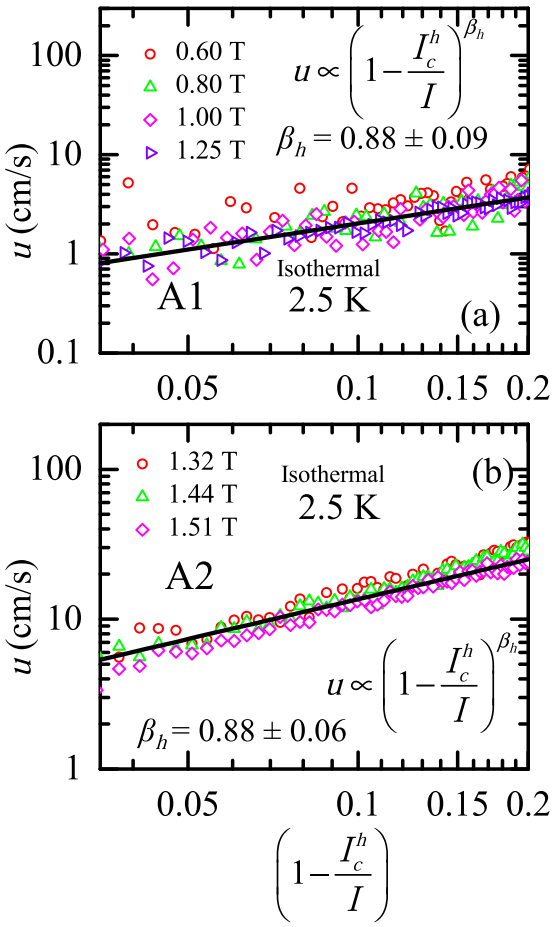

FIG. 4. Panels (a) and (b) show u vs $(1-\frac{I_c^h}{I})$ in log-log scale at 2.5 K for various B's for samples A1 and A2 respectively, estimated from IV data [see Fig. 1(c) main panel for sample A1]. The thick black lines are fit to the equation $u \propto (1-\frac{I_c^h}{I})^{\beta_h}$ with $\beta_h = 0.88 \pm 0.09$ for sample A1 and 0.88 ± 0.06 for A2.

of the Fisher's scaling form which is valid for depinning at absolute zero. The above suggests that the NEQ vortex phase with I_c^h is unaffected by thermal fluctuation effects. Here, we would like to recall the scaling schemes for analyzing IV proposed by Fisher, Fisher, and Huse [29]. This scheme investigates conductivity fluctuations and determines dynamic exponents through transport measurements performed near T_c. In superconductors, a parameter which controls the width of the thermal fluctuations dominated regime around $T_c(H)$ is the Ginzburg number G_i [15]. Using values of T_c, upper critical field B_{c2}, κ, and superconducting coherence length ξ reported in Ref. [40], we estimate for $2H$-NbS_2 $G_i \sim 2 \times 10^{-3}$, which is similar to that of low-T_c superconductor $2H$-$NbSe_2$ and about one to two orders of magnitude smaller than that of high-T_c superconductors. Therefore, the thermal fluctuation dominated regime is extremely narrow in this superconductor and is restricted to a region very close to T_c. Based on our above discussion, we estimate that the critical thermal fluctuation regime in the vortex matter phase diagram for $2H$-NbS_2 would be located between the upper-critical field line and the irreversibility line, viz., see the region marked as "reversible" in Sec. (iv) of the Supplemental Material [39]. Typically, this reversible critical fluctuation regime would be within $0.9T_c$, however we have performed our measurements at $T \ll 0.9T_c$, viz., in a regime well outside the critical fluctuation regime. Due to the above we analyze our IV data over a wide temperature and field range using the scaling schemes in Refs. [30,32] which are applicable over a wider range of temperature. The above also shows that as we find I_c^h states at temperature regions well outside the critical fluctuation regime, this also reconfirms our argument that the abrupt drop in IV near I_c^h isn't related to critical thermal fluctuations. It may be noted that a high I_c^h value is only associated with the vortex phase generated via an abrupt drop in vortex velocity when it is driven with large currents; it is not reached by any other conventional means of preparing the static vortex lattice, viz., by subjecting the superconductor to different thermomagnetic history (field cooling or zero-field cooling or pulsing field or temperature, etc.) while creating the static vortex lattice. An important characteristic of the dynamically generated I_c^h vortex phase is that it exhibits the ability to withstand the destabilizing influence of thermal fluctuations without diminishing the depinning threshold. Such a feature is difficult to generate in any superconductor with intrinsic pinning, as the conventionally pinned vortex state is always prone to thermal fluctuation effects which diminish the effective pinning potential. Even in the vortex state in superconductors with artificial pinning centers (generated by heavy ion irradiation and nanopatterning) it is difficult to avoid the ubiquitous effects of thermal fluctuations, as thermally activated behavior is observed even in such systems. In this respect it is interesting to note that we show that the high I_c^h states generated from instabilities in a fast moving vortex state are stable against the destabilizing influence of the effects of thermal fluctuations which lead to a lowering of the critical current. Such dynamically generated vortex states could have application potential. Our work also suggests the vortex state at I_c^h is peculiar and different from the conventional I_c^l. In the next section, we explore the circumstances in which the I_c^h state is generated a bit more closely.

VIII. SIGNATURES OF NDR TRANSITION AND TRANSFORMATION TO THE I_c^h STATE

The IV data shown in Fig. 1(c) inset has been replotted in Fig. 5(a), in terms of the variation of the normalized resistivity, $\frac{\rho}{\rho_f}$, with I, where ρ is the resistivity of the dissipating moving vortex state, $\rho_f = \rho_n \frac{B}{B_{c2}}$ is the Bardeen-Stephen flux flow resistivity [15,54], $\rho_n = 60\,\mu\Omega\,\text{cm}$ is the normal-state resistivity of sample A1, B_{c2} is the upper critical field which is 2.5 T (at 2.5 K) for sample A1 and 2.6 T (at 2.5 K) for A2. The estimated values of ρ_f for A1 at 0.2 and 0.7 T (with $T = 2.5$ K) are 4.8 and 16.8 $\mu\Omega\,\text{cm}$ respectively. As already discussed in Fig. 1(c) inset, in Fig 5(a) we observe that for the forward run as I is increased, after depinning from the static vortex mater at $I_c^l \sim 25$ mA, $\frac{\rho}{\rho_f}(I)$ (or dissipation) exhibits a change in curvature at $I_{\text{cr}} \sim 32$ mA. As already discussed, the I_{cr} signals the transformation of the moving vortex state from a thermally activated to free flow regime. In this regime the dissipation becomes almost constant. Note in this steady flow regime above I_{cr} the value of $\frac{\rho}{\rho_f} \sim 9$, which is significantly higher than

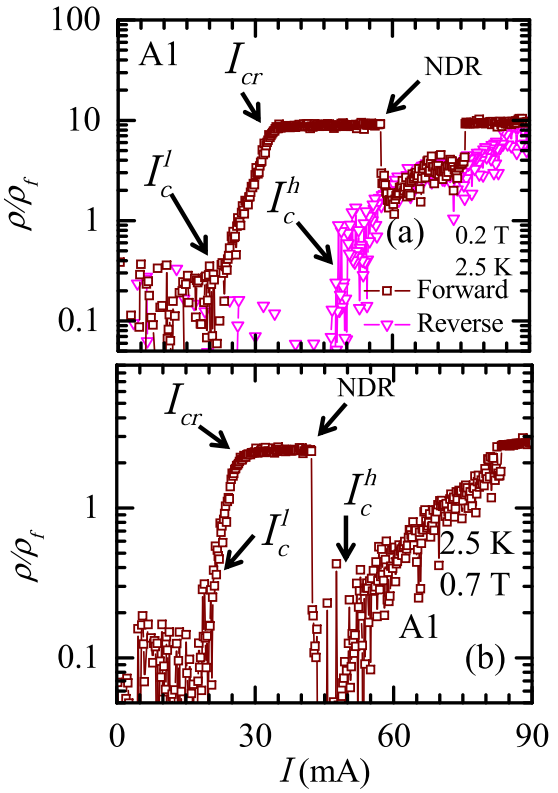

FIG. 5. (a),(b) Isothermal $\frac{\rho}{\rho_f}(I)$ response in log linear scale for sample A1 measured at 2.5 K with $B = 0.2$ and 0.7 T respectively. The locations of I_c^l,$I_{\rm cr}$, and I_c^h have been marked with arrows.

the Bardeen-Stephen flux flow limit of 1. This steady flow state with elevated $\frac{\rho}{\rho_f}$ value is sustained up to 60 mA after which the dissipation abruptly drops. Earlier studies have shown that in the fast moving vortex states when $\frac{\rho}{\rho_f} > 1$ the onset of high dissipation triggers instabilities in vortex dynamics leading to an abrupt fall in vortex velocity, viz., the onset of a negative differential resistance (NDR) transition [46–52]. Theoretical studies in the NDR regime [46,49–52] suggest S- or N-shaped instabilities developing in the *IV* due to the abrupt fall or increase in vortex velocity. Note that in Fig. 5(a) we see evidence of this instability associated with NDR as the abrupt drop in the vortex dissipation at 60 mA is followed by an equally abrupt rise in dissipation at 75 mA. In the reverse *IV* run, the dissipation fluctuates and settles below the noise floor at I less than a critical value of $I_c^h \sim 45$ mA. By comparing the forward and reverse runs above 50 mA [brown and pink curves in Fig. 5(a) and inset of Fig. 1(c)] a hysteresis in *IV* is clearly discernible. It had been predicted that such a hysteretic *IV* exists due to instabilities in the vortex dynamics in the NDR regime [46,49–52] (note that in sample A2 an example of such a hysteresis in *IV* is seen in Fig. 2 of Ref. [36]).

In Fig. 5(b) note that above $I_{\rm cr}$, $\frac{\rho}{\rho_f}$ is lower than that at 0.2 T as ρ_f has increased by 3.5 times as B increases from 0.2 to 0.7 T. Note that at 0.7 T the NDR drop occurs much earlier than at 0.2 T, although $\frac{\rho}{\rho_f}$ is lower. The most striking difference between the behavior of the forward runs in Figs. 5(a) and 5(b) is that, at 0.7 T after the onset of NDR, the dissipation or the vortex velocity abruptly drops below the noise floor. Furthermore, from Fig. 5(b) we see that at 0.7 T depinning occurs at $I_c^h \sim 45$ mA which is followed by fluctuation in the vortex velocity [as observed at 0.2 T as well in Fig. 5(a)]. Hence from Figs. 5(a) and 5(b), we see that at moderately higher B (∼0.7 T) the high I_c state is reached with the forward run itself. It may be mentioned here that sufficiently strong pinning is known to suppress the NDR dynamic instability [49]. The features in Fig. 5(b) suggest that the instabilities in the vortex dynamics lead to an NDR transition and this transition is favorable at higher vortex densities (or B). This NDR state depins only at a higher drive (I_c^h) which we show is independent of B and T [see Figs. 1(c) and 1(d)] suggesting pinning or thermal fluctuations don't affect the depinning at I_c^h, which is unlike the nature of depinning at I_c^l. It is clear from the above study that fluctuations above I_c^h are not related to thermal fluctuations but rather with instabilities in the NDR regime.

IX. DISCUSSION AND CONCLUSIONS

Recall that the scaling relation of Eq. (7) suggests $u \propto \frac{1}{n}$, namely, increasing vortex density (n) leads to a reduction in the vortex velocity (u). It appears that enhanced intervortex interactions impede vortex motion possibly due to enhanced caging potential created by mutually repelling neighboring vortices at high n. Presumably, the NDR instability generates significant density fluctuations in the moving vortex state. Locally, in regions with higher vortex density the velocity of the vortex state would be lowered (due to $u \propto \frac{1}{n}$). This local slowing down would in turn generate more density fluctuations in the state. The net recursive effect would quickly bring the entire vortex state down to a lower velocity state and produce the sharp drop in u [as seen in Fig. 1(c) inset and Fig. 5]. Our earlier measurements [36,37] have shown that depinning at I_c^h is accompanied by unusually large fluctuations in u which are sustained for a characteristic time scale τ_h. The τ_h exhibits a diverging relationship with the driving force of the form $\tau_h \propto \frac{1}{|I-I_c^h|^\zeta}$ [see Fig. 4 of Ref. [36] and also Fig. S4(c) of Ref. [37]]. The value of the exponent ζ suggested a universality class associated with this NEQ transition. This feature for the NEQ transition at I_c^h is in fact similar to the critical slowing down of kinetics near an equilibrium critical point (critical temperature). Along with the above similarity, like equilibrium critical phase transition phenomena, NEQ transformations also exhibit a scaling relationship between the velocity and drive across I_c^h. All these unique features associated with the I_c^h state suggest we can identify it as a distinct NEQ phase acquired through the NDR transition at high drives.

Depinning at I_c^h, which obeys the Fisher's scaling expression Eq. (1) [30,31], shows an abrupt increase in vortex velocity (u) at the depinning threshold. This abrupt increase in u reaffirms the original proposal of Fisher to treat u like an order parameter for the NEQ depinning, based on which Eq. (1) was proposed. This behavior of u also suggests a coherent nature of depinning of the entire vortex state at I_c^h. Thus, although the vortex state at I_c^h is likely to be disordered (as it possesses a higher I_c), it appears to depin coherently like a rigid elastic solid-like phase (as it obeys Fisher's scaling form, which was proposed for depinning of an interacting ordered elastic medium at 0 K). Additionally, although the vortex lattice depins coherently at I_c^h, after depinning the

driven vortex matter exhibits significant velocity fluctuations (which we have shown earlier are not related to thermal fluctuations). We would like to mention that the velocity fluctuations we observe in the driven vortex state are not due to thermal fluctuations ($G_i \sim 10^{-3}$ in $2H$-NbS_2). We believe above I_c^h the disordered vortex state in the NDR regime has flow instabilities which lead to noise in vortex velocity. This noisy regime has been explored recently, where fluctuations in the vortex velocity in time series measurements above I_c^h exhibit interesting connections with nonequilibrium fluctuation relationships [37,55]. Here it may be worth recalling that similar fluctuations have been observed while driving jammed granular/colloidal systems [56–60]. It was shown that these fluctuations are also not related to thermal fluctuations [60]. The noise associated while unjamming these granular/colloidal systems was shown to obey Gallavotti-Cohen nonequilibrium fluctuation relations [60,61]. While vortices are distinct from granular or colloidal particles, some of the properties of their NEQ phases seem similar. Based on the above similarities of noise features with those we observe for the vortex depinning phenomena above I_c^h, we are tempted to speculate that a nonequilibrium drive induced jammed vortex configuration may be produced via the NDR instability. Depinning of such a NEQ phase at zero temperature follows the predicted Fisher form [30]. While conventional depinning exhibits a thermally activated regime of vortex flow, depinning from I_c^h is a distinct transition.

To conclude, we have used the vortex depinning characteristics in $2H$-NbS_2 single crystals as a prototype to study nonequilibrium phases and NEQ phase transitions. We identify the relevant order parameter which is the vortex velocity associated with the NEQ depinning phase transitions and the scaling relationships it obeys. We show how the order parameter is modified by the effects of temperature and density of vortices. We show the scaling parameters are sensitive to the dimensionality of the system. We use this analysis to quantitatively understand the inflexion in the *IV* curve which has often been seen in many experiments in the past. We study properties of an unusual NEQ driven vortex phase generated from an unstable high velocity flow regime. The properties of this NEQ vortex phase with a high critical current are unlike that of a conventional pinned state. By analogy we propose the high-I_c state has properties akin to the NEQ jammed phase found in different systems with arrested kinetics. We hope that this unusual NEQ vortex phase generated from an unstable vortex flow state will provide a way to access high critical-current states of a superconductor which conventionally are not accessible. Future theoretical and experimental investigations are needed to unravel the nature of this nonequilibrium vortex phase with high critical current with unusual flow properties upon depinning.

ACKNOWLEDGMENTS

S.S.B. acknowledges IIT Kanpur-India, Department of Science and Technology (TSDP) India, for funding support, as well as discussions with Professor X. Hu of NIMS Japan on analysis of the *IV*'s with low I_c.

[1] P. M. Chaikin and T. C. Lubensky, *Principles of Condensed Matter Physics* (Cambridge University Press, Cambridge, England, 1995).
[2] H. E. Stanley, Rev. Mod. Phys. **71**, S358 (1999).
[3] A. Arrott and J. E. Noakes, Phys. Rev. Lett. **19**, 786 (1967).
[4] B. Liu, Y. Zou, L. Zhang, S. Zhou, Z. Wang, W. Wang, Z. Qu, and Y. Zhang, Sci. Rep. **6**, 33873 (2016).
[5] J. P. Golub and J. S. Langar, Rev. Mod. Phys. **71**, S396 (1999).
[6] L. Berthier and J. Kurchan, Nat. Phys. **9**, 310 (2013).
[7] G. Dagvadorj, J. M. Fellows, S. Matyjaśkiewicz, F. M. Marchetti, I. Carusotto, and M. H. Szymańska, Phys. Rev. X **5**, 041028 (2015).
[8] H. Hinrichsen, Adv. Phys. **49**, 815 (2000).
[9] G. Odor, Rev. Mod. Phys. **76**, 663 (2004).
[10] C. Reichhardt and C. J. Olson Reichhardt, Rep. Prog. Phys. **80**, 026501 (2017).
[11] A. Maeda, M. Notomi, and K. Uchinokura, Phys. Rev. B **42**, 3290 (1990).
[12] M. Mu¨ller, D. A. Gorokhov, and G. Blatter, Phys. Rev. B **63**, 184305 (2001).
[13] C. Reichhardt and C. J. Olson Reichhardt, Phys. Rev. Lett. **103**, 168301 (2009), and references therein.
[14] A. Pertsinidis and X. S. Ling, Phys. Rev. Lett. **100**, 028303 (2008).
[15] G. Blatter, M. V. Feigel'man, V. B. Geshkenbein, A. I. Larkin, and V. M. Vinokur, Rev. Mod. Phys. **66**, 1125 (1994).
[16] T. Giammarchi and S. Bhattacharya, Vortex Phases, in *High Magnetic Fields: Applications in Condensed Matter Physics and Spectroscopy*, edited by C. Berthier, L. P. Levy, and G. Martinez (Springer, Berlin, 2001), pp. 314–360, and references therein.
[17] S. Scheidl and V. M. Vinokur, Phys. Rev. E **57**, 2574 (1998).
[18] D. J. Pine, J. P. Gollub, J. F. Brady, and A. M. Leshansky, Nature (London) **438**, 997 (2005).
[19] E. C. Eckstein, D. G. Bailey, and A. H. Shapiro, J. Fluid Mech. **79**, 191 (1977).
[20] V. Breedveld, D. van den Ende, R. Jongschaap, and J. Mellema, J. Chem. Phys. **114**, 5923 (2001).
[21] G. Drazer, J. Koplik, B. Khusid, and A. Acrivos, J. Fluid Mech. **511**, 237 (2004).
[22] L. Corte, P. M. Chaikin, J. P. Gollub, and D. J. Pine, Nat. Phys. **4**, 420 (2008).
[23] C. Zhou, C. Reichhardt, C. J. O. Reichhardt, and I. J. Beyerlein, Sci. Rep. **5**, 8000 (2015)
[24] M. J. Higgins and S. Bhattacharya, Physica C **257**, 232 (1996).
[25] A. E. Koshelev and V. M. Vinokur, Phys. Rev. Lett. **73**, 3580 (1994).
[26] P. Le Doussal and T. Giamarchi, Phys. Rev. B **57**, 11356 (1998).
[27] L. Balents, C. M. Marchetti, and L. Radzihovsky, Phys. Rev. Lett. **78**, 751 (1997).
[28] F. Pardo, F. de la Cruz, P. L. Gammel, E. Bucher, and D. J. Bishop, Nature (London) **396**, 348 (1998).
[29] D. S. Fisher, M. P. A. Fisher, and D. A. Huse, Phys. Rev. B **43**, 130 (1991).
[30] D. S Fisher, Phys. Rev. B **31**, 1396 (1985).

[31] P. Chauve, T. Giamarchi, and P. Le Doussal, Phys. Rev. B **62**, 6241 (2000).

[32] M. B. Luo and X. Hu, Phys. Rev. Lett. **98**, 267002 (2007).

[33] Y. Fily, E. Olive, N. D. Scala, and J. C. Soret, Phys. Rev. B **82**, 134519 (2010).

[34] B. Xi, M. B. Luo, V. M. Vinokur, and X. Hu, Sci. Rep. **5**, 14062 (2015).

[35] S. Okuma, A. Motohashi, and Y. Kawamura, Supercond. Sci. Technol. **26**, 025013 (2013).

[36] G. Shaw, P. Mandal, S. S. Banerjee, A. Niazi, A. K. Rastogi, A. K. Sood, S. Ramakrishnan, and A. K. Grover, Phys. Rev. B **85**, 174517 (2012).

[37] B. Bag, G. Shaw, S. S. Banerjee, S. Majumdar, A. K. Sood, and A. K. Grover, Sci. Rep. **7**, 5531 (2017).

[38] A. Niazi and A. K. Rastogi, J. Phys.: Condens. Matter **13**, 6787 (2001); A. Niazi, Ph.D. thesis, School of Physical Sciences, Jawaharlal Nehru University, New Delhi, India, 1999.

[39] See Supplemental Material at http://link.aps.org/supplemental/10.1103/PhysRevB.97.134510 for seven sections: (i) isothermal IV, data measured for the FC vortex state; (ii) IV characteristics across I_c^l for sample A1 with V axis in log scale; (iii) IV characteristics across I_c^l for sample A2; (iv) order-to-disorder transition in the static vortex state at the onset of SMP anomaly; (v) fluctuation in temperature and issue of contact-heating during IV measurement; (vi) scaling of isofield IV curves for different $\beta_l\delta$ values; (vii) scaling of isofield IV curves across I_c^h for sample A1.

[40] A. A. Tulapurkar, A. K. Grover, S. Ramakrishnan, A. Niazi, and A. K. Rastogi, Physica B **312-313**, 118 (2003).

[41] A. I. Larkin and Y. N. Ovchinnikov, J. Low Temp. Phys. **34**, 409 (1979).

[42] L. A. Angurel, F. Amin, M. Polichetti, J. Aarts, and P. H. Kes, Phys. Rev. B **56**, 3425 (1997).

[43] J. R. Clem, in *Proceedings of 13th Conference on Low Temperature Physics (LT 13)*, edited by K. D. Timmerhaus, W. J. O'Sullivan, and E. F. Hammel (Plenum, New York, 1974), Vol. 3, p. 102.

[44] P. K. Mishra, G. Ravikumar, T. V. Chandrasekhar Rao, V. C. Sahni, S. S. Banerjee, S. Ramakrishnan, A. K. Grover, and M. J. Higgins, Physica C **340**, 65 (2000).

[45] S. Mohan, J. Sinha, S. S. Banerjee, and Y. Myasoedov, Phys. Rev. Lett. **98**, 027003 (2007).

[46] R. G. Mints and A. L. Rakhmanov, Rev. Mod. Phys. **53**, 551 (1981).

[47] M. N. Kunchur, B. I. Ivlev, D. K. Christen, and J. M. Knight, Phys. Rev. Lett. **84**, 5204 (2000).

[48] M. N. Kunchur, B. I. Ivlev, and J. M. Knight, Phys. Rev. Lett. **87**, 177001 (2001).

[49] C. Reichhardt, C. J. O. Reichhardt, and F. Nori, Phys. Rev. Lett. **78**, 2648 (1997).

[50] C. Reichhardt, C. J. O. Reichhardt, and F. Nori, Phys. Rev. B **58**, 6534 (1998).

[51] V. R. Misko, S. Savel, A. L. Rakhmanov, and F. Nori, Phys. Rev. Lett. **96**, 127004 (2006).

[52] V. R. Misko, S. Savel'ev, A. L. Rakhmanov, and F. Nori, Phys. Rev. B **75**, 024509 (2007).

[53] M. Daeumling, J. M. Seuntjens, and D. C. Larbalestier, Nature (London) **346**, 332 (1990); M. F. Goffman, Phys. Rev. B **57**, 3663 (1998), and references therein; S. S. Banerjee *et al.*, *ibid.* **62**, 11838 (2000); D. Pal, S. Ramakrishnan, and A. K. Grover, *ibid.* **63**, 132505 (2001); N. Avraham *et al.*, Nature (London) **411**, 451 (2001); M. Zehetmayer, Sci. Rep **5**, 9244 (2015).

[54] J. Bardeen and M. J. Stephen, Phys. Rev. **140**, A1197 (1965).

[55] G. M. Wang, E. M. Sevick, E. Mittag, D. J. Searles, and D. J. Evans, Phys. Rev. Lett. **89**, 050601 (2002); J. Gieseler, R. Quidant, C. Dellago, and L. Novotny, Nat. Nanotechnol. **9**, 358 (2014); N. Garnier and S. Ciliberto, Phys. Rev. E **71**, 060101 (2005); D. Collin, F. Ritort, C. Jarzynski, S. B. Smith, I. Tinoco Jr., and C. Bustamante, Nature (London) **437**, 231 (2005); J. Liphardt, S. Dumont, S. B. Smith, I. Tinoco Jr., and C. Bustamante, Science **296**, 1832 (2002).

[56] A. J. Liu and S. R. Nagel, Nature (London) **396**, 21 (1998).

[57] C. Reichhardt and C. J. O Reichhardt, Soft Matter **10**, 2932 (2014).

[58] C. Reichhardt and C. J. O Reichhardt, Phys. Rev. B **78**, 224511 (2008).

[59] C. J. O Reichhardt and C. Reichhardt, Phys. Rev. B **81**, 224516 (2010).

[60] S. Majumdar and A. K. Sood, Phys. Rev. Lett. **101**, 078301 (2008).

[61] N. Kumar, S. Ramaswamy, and A. K. Sood, Phys. Rev. Lett. **106**, 118001 (2011).